Available online at www.sciencedirect.com
ScienceDirect
Ceramics International 38 (2012) 541–545
CERAMICS INTERNATIONAL
www.elsevier.com/locate/ceramint

Preparation and characterization of negative thermal expansion $Sc_2W_3O_{12}$/Cu core–shell composite

Qinqin Liu *, Juan Yang, Xiaonong Cheng, Guoshan Liang, Xiujuan Sun

School of Materials Science and Engineering, Jiangsu University, 301 Xuefu Road, Zhenjiang, Jiangsu 212013, PR China

Received 16 June 2011; received in revised form 21 July 2011; accepted 21 July 2011
Available online 28th July 2011

Abstract

A composite of $Sc_2W_3O_{12}$/Cu where $Sc_2W_3O_{12}$, the core, is coated by the Cu shell was synthesized using simple electroless plating method. As-prepared $Sc_2W_3O_{12}$/Cu composites were characterized by X-ray diffraction (XRD), scanning electron microscopy (SEM), energy dispersive spectrometry (EDS) and thermomechanical analyzer (TMA) techniques. The study results show that the Pd–Sn activator was successfully formed on the surface of $Sc_2W_3O_{12}$ after the sensitization and activation. In the electroless plating process, Cu nanocrystals formed firstly, and then grew together to form a continuous coating. $Sc_2W_3O_{12}$/Cu core–shell composites exhibit a negative linear coefficient of thermal expansion CTE = $-4.47 \times 10^{-6}\ ^{\circ}C^{-1}$ from room temperature to 200 °C.

Keywords: $Sc_2W_3O_{12}$/Cu composite; Core–shell structure; Negative thermal expansion

1. Introduction

Copper matrix composites (CMCs) consisting of a metallic matrix (Cu) with high thermal conductivity and a ceramic reinforcement (SiC [1], AlN [2], TiB_2 [3,4], and β-eucryptite [5]) with low coefficient thermal expansion (CTE) provide exceptional freedom in tailoring these two properties to specific application [6]. For example, application for thermal management systems in electronics (e.g. expansion matched to substrate while maximizing conductivity for electronic heat sinks) [7].

Since generally increasing the ceramic content of composite decreases both of thermal conductivity and thermal expansion, ceramic with a negative CTE is a promising candidates as reinforcement to maximize the conductivity/expansion ratio of the composite. Cubic ZrW_2O_8 is the most well-known negative thermal expansion (NTE) material, as it displays isotropic NTE over a large temperature range (−273 to 777 °C) [8]. Dunand [9] had tried to combine it with copper to develop composite with high thermal conductivity and controlled CTE. Unfortunately, ZrW_2O_8/Cu composite exhibited very large dilatometric expansion on heating and contraction on cooling, much above those predicted from thermo-elasticity theory [10]. This unexpected result was proved to be caused by the formation of the high-pressure γ-ZrW_2O_8 phase from the ambient pressure α-ZrW_2O_8 phase at about 0.4 GPa [11] (or β-ZrW_2O_8 phase above 423 K [12]).

$Sc_2W_3O_{12}$ as another typical NTE material shows stronger negative thermal expansion (CTE of its ceramic bar is $-11 \times 10^{-6}\ ^{\circ}C^{-1}$) than that shown by ZrW_2O_8, and its NTE behavior continues from room temperature to 927 °C (the upper temperature limit of their equipment [13]) and ∼11 GPa [14]. No phase transitions are observed in this temperature range, and the higher onset transition pressure might be advantageous for its applications in CMCs composites. Few literatures about $Sc_2W_3O_{12}$-containing CMCs composites had been reported thus far.

In this paper, $Sc_2W_3O_{12}$/Cu composites with core–shell structure were prepared. Electroless coating technology (instead of an admixture method) was utilized to enhance the compatibility between ceramic and metal component. The structure, morphology and thermal expansion property of the as-prepared samples were studied.

* Corresponding author. Tel.: +86 511 88780195; fax: +86 511 88791947.
E-mail address: liu_qin_qin@126.com (Q. Liu).

0272-8842/$36.00
doi:10.1016/j.ceramint.2011.07.041

2. Experimental

2.1. Preparation of $Sc_2(WO_4)_3$

$Sc_2W_3O_{12}$ powders were prepared using solid state method. Stoichiometric Sc_2O_3 and WO_3 were thoroughly mixed and ground, then the mixture was calcined at 900 °C for 30 h in air.

2.2. Preparation of $Sc_2W_3O_{12}$/Cu core–shell composite

Before electroless plating, surface treatment was carried out on the $Sc_2W_3O_{12}$ powders. Firstly, the $Sc_2W_3O_{12}$ powders were immersed in a HCl solution (20 wt%) with ultrasonic cleaning for 2 min. After that the $Sc_2W_3O_{12}$ powders were sensitized in a $SnCl_2$ solution (20 wt%) with ultrasonic processing for 5 min, and then activated in a $PdCl_2$ solution (3 wt%) with ultrasonic processing for 30 min.

The activated $Sc_2W_3O_{12}$ powders were transferred into the electroless copper coating bath solution with a pH of 12 at room temperature, and ultrasonic processing for coating 2 h. The pH was adjusted with 5 wt% NaOH solution. The Cu-coated $Sc_2W_3O_{12}$ powders were cleaned by distilled water several times until the pH value of the water was equal to 7, and dried at 60 °C. The dried Cu-coated $Sc_2W_3O_{12}$ powders were ground and pressed into a cylinder at 20 MPa with the size of Φ5 mm × 30 mm, then the cylinder was heated at 1000 °C for 6 h in argon atmosphere.

The composition of the coating bath was as follows: 25 g/L of $CuSO_4{\cdot}5H_2O$, 12.5 mL of HCHO (37 wt%), 90 g/L of $KNaC_4H_4O_4{\cdot}4H_2O$, 25 g/L of NaOH, 62 mg/L of $K_4Fe(CN)_3$ and 16 mg/L of 2,2′-dipyridyl, $C_{10}H_8N$.

2.3. Characterization

The products were characterized by X-ray powder diffraction (XRD) analysis (D/max-2500, Rigaku, Japan) using Cu-Kα radiation (λ = 0.15406 nm) with 40 kV/200 mA. The XRD patterns were collected between $2\theta = 10^\circ$ and $2\theta = 70^\circ$ with a scan speed of 5° min^{-1}. Morphological characterization was carried out by Field Emission Scanning Electron Microscopy (FE-SEM) using a JSM-7001F JEOL (Japan) microscope equipped with EDS. The thermal expansion coefficients were measured by thermomechanical analyzer (TMA, NETZSCH DIL 402EP, Selb, Germany) using the cylinder specimen.

3. Results and discussion

The XRD pattern of the as-prepared $Sc_2W_3O_{12}$ is shown in Fig. 1a. The powder X-ray diffraction pattern of the material proved its crystalline nature and the peaks matched well with standard $Sc_2W_3O_{12}$ reflections (JCPDS: 21-1065) [14]. Fig. 1b shows the XRD pattern of the Cu-coated $Sc_2W_3O_{12}$ powders. No reflection could be discerned other than the (1 1 1) and (2 0 0) diffraction peaks of Cu (JCPDS: 04-0836) with *f c c* structure, implying that a thick layer of Cu was deposited on the surface of $Sc_2W_3O_{12}$.

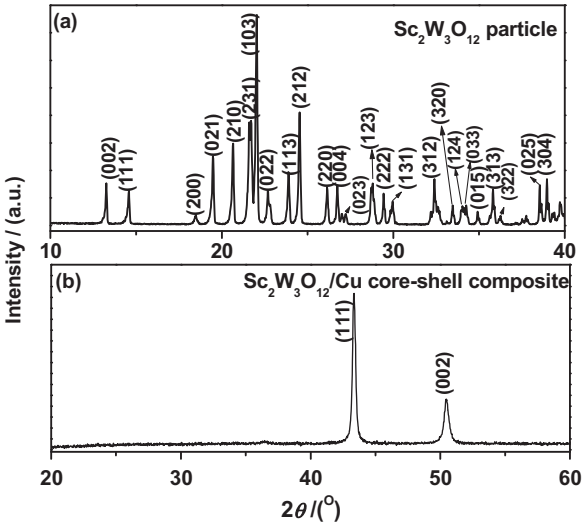

Fig. 1. XRD patterns of (a) the $Sc_2W_3O_{12}$ powders and (b) $Sc_2W_3O_{12}$/Cu core–shell composite powders.

SEM micrographs of $Sc_2W_3O_{12}$ and Cu-coated $Sc_2W_3O_{12}$ powders are presented in Fig. 2. The morphology seen in Fig. 2a is the typical irregular $Sc_2W_3O_{12}$ particles with the average size about 1–1.5 μm, it is found in further observations that some particles conglutinate to each other due to the high sintering temperature. In Fig. 2b, all the $Sc_2W_3O_{12}$ particles are observed to be homogeneously coated with Cu particles by the present electroless technique. It is to be noted that the Cu-coated $Sc_2W_3O_{12}$ particles also exhibit the irregular morphology, suggesting that Cu crystallites with diameters of 200 nm are absorbed into the surfaces of $Sc_2W_3O_{12}$ particles by physical bonding. Even though the physical bonding types between the $Sc_2W_3O_{12}$ and Cu particles are not now fully understood, one of which Van der Waals' forces may function. When settling nano-sized Cu crystallites are in contact with rigid surfaces of the $Sc_2W_3O_{12}$ particles, an instantaneous shear strain might possibly occur at the surface of Cu particle due to the combined effects of relative sliding and the ductility of the nano Cu crystallites [15]. Fig. 2c shows high-magnifications SEM micrograph of the Cu-coated $Sc_2W_3O_{12}$, it is evident that there was a relatively continuous, dense and uniform layer of Cu on the surface of all the $Sc_2W_3O_{12}$ particles, so was there on the small amount of debris. EDS of $Sc_2W_3O_{12}$ and Cu-coated $Sc_2W_3O_{12}$ powder are presented in Fig. 2e and f. The EDS spectrum of $Sc_2W_3O_{12}$ is composed of Sc, W and O with atomic ratio of 2:2.97:12.74, close to the stoichiometric ratio; while the Cu-coated $Sc_2W_3O_{12}$ as indicated by Fig. 2e mainly consisted of Cu. It should be noted that the peaks corresponding to Cu were not detected in the as-prepared $Sc_2W_3O_{12}$, and they appeared only after the electroless coating process, indicating successful Cu deposition on the $Sc_2W_3O_{12}$ surface and the formation of $Sc_2W_3O_{12}$/Cu core–shell composite by the present electroless technique.

The density of the $Sc_2W_3O_{12}$/Cu core–shell composite powders calculated by measuring the mass and volume was about 5.13 g/cm^3. The average specific volume resistivity, obtained by the four probe method, was 153.4 K Ω^{-1} for

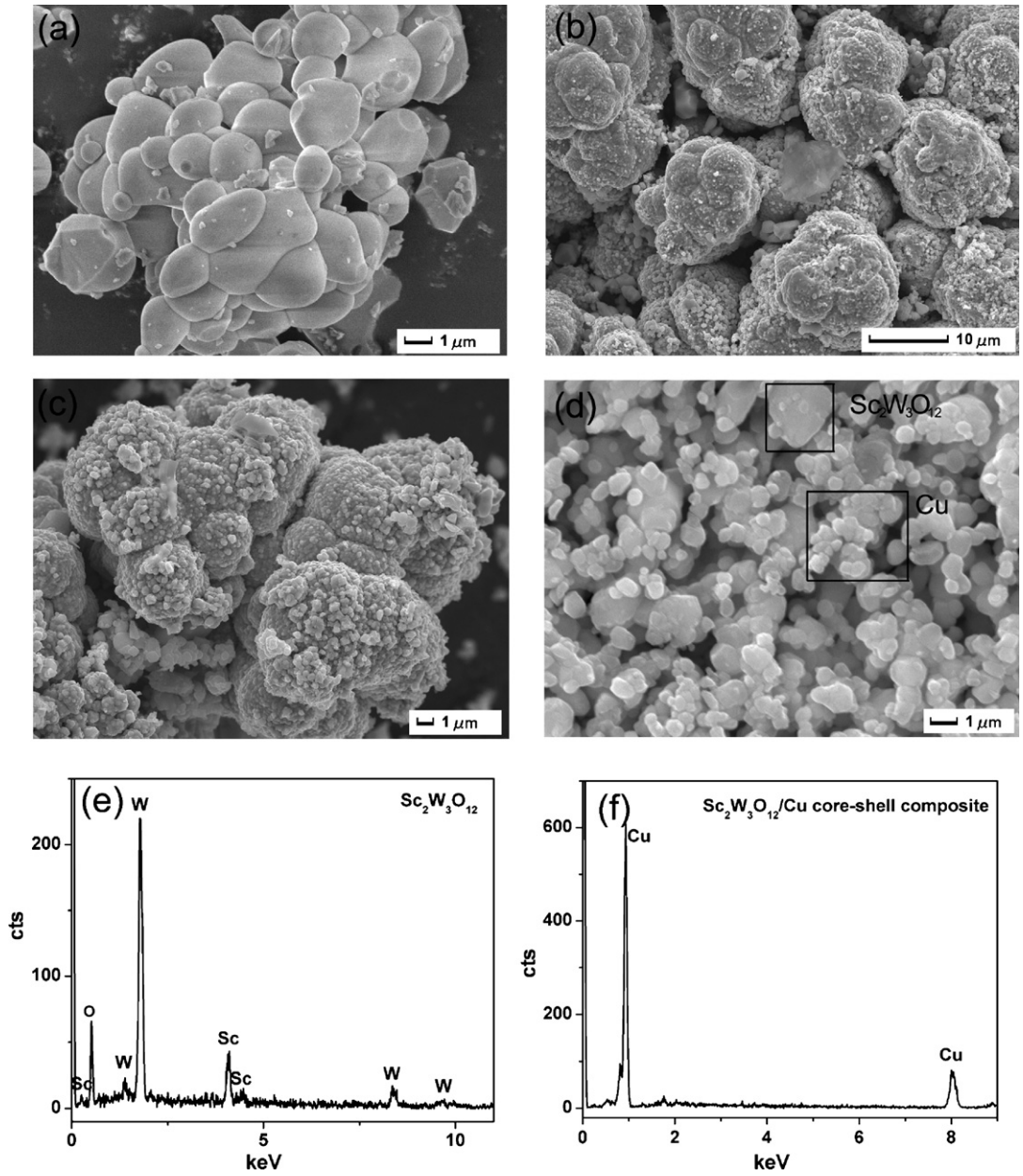

Fig. 2. SEM micrographs of (a) $Sc_2W_3O_{12}$ powders, (b) and (c) $Sc_2W_3O_{12}$/Cu core–shell composite powders at different magnifications, (d) the obtained products by coating $Sc_2W_3O_{12}$ without sensitization and activation, (e) EDS analysis of the $Sc_2W_3O_{12}$ powders and (f) $Sc_2W_3O_{12}$/Cu core–shell composite powders.

$Sc_2W_3O_{12}$ and 345.78 Ω^{-1} for the $Sc_2W_3O_{12}$/Cu core–shell composite. This great decrease in the specific resistivity confirms that the $Sc_2W_3O_{12}$ was covered by the copper.

It is known that the electroless coating process is an autocatalytic redox reaction [16]. The beginning of the copper deposition is controlled by the anodic processes, and Pd was usually thought as the active catalyst in electroless plating process [17]. In order to investigate the role of Pd, the $Sc_2W_3O_{12}$ powders without sensitization and activation were used in the same electroless copper coating bath, and the SEM image of the resulting product is shown in Fig. 2d. Its morphology is greatly different from that obtained after sensitization and activation; the product consists of two different sizes of particles. According to EDS results, the larger one is $Sc_2W_3O_{12}$ and the smaller one is Cu. The nucleation of the Cu randomly formed in the solution rather than on the surface of $Sc_2W_3O_{12}$ particles under this condition, so $Sc_2W_3O_{12}$/Cu core–shell structure only can be obtained in the presence of catalyst Pd.

Based on the above XRD, SEM and EDS analyses, we suggest that the possible mechanism of electroless copper plating of $Sc_2W_3O_{12}$ powder is as follows.

First, Sn^{2+} was adsorbed uniformly on the surface of $Sc_2W_3O_{12}$ by the static force when $Sc_2W_3O_{12}$ powder was transferred to the sensitization solution. This is very important to form the Pd–Sn catalytic core in the activation processing. In the present work, the activation was completed in the $PdCl_2$ solution. Hence, the Pd^{2+} and Sn^{2+} should react following

equation (Eq. (1)):

$$Pd^{2+} + Sn^{2+} \rightarrow Pd + Sn^{4+} \quad (1)$$

The Pd–Sn catalytic core facilitates conditions for electroless plating. $Sc_2W_3O_{12}$ after sensitization and activation were put into the plating solution, Cu^{2+} get deposited on Pd–Sn catalytic core surface by capturing electrons furnished by reducing agent (HCHO) via the following chemical reactions:

Anodic reaction

$$: \quad 2HCHO + 4OH^- \rightarrow H^{2+} + 2HCOO^- + H_2O + 2e^- \quad (2)$$

$$\text{Cathodic reaction} : \quad Cu^{2+} + 2e^- \rightarrow Cu \quad (3)$$

The overall reaction can be written as:

$$Cu^{2+} + 2HCHO + 4OH^- \rightarrow Cu\downarrow + H^{2+}\uparrow + 2HCOO^- + H_2O \quad (4)$$

Firstly, Cu nanoparticles are formed after nucleation, then, the superfluous Cu^{2+} ions in the solution would be adsorbed on the Cu nanoparticles to form bigger particles. These Cu particles contact with $Sc_2W_3O_{12}$ since the copper reduction occurs on the $Sc_2W_3O_{12}$ surface. Hence the $Sc_2W_3O_{12}$–Cu core–shell structure is formed.

The dependence of thermal expansion and thermal expansion coefficient on temperature of $Sc_2(WO_4)_3$ and $Sc_2W_3O_{12}$/Cu core–shell composite were measured with a dilatometer, and the results are shown in Fig. 3. The CTE ($\alpha(T)$) was calculated by using Eq. (5) [16]:

$$\alpha(T) = \frac{1}{L(T)}\frac{\partial L(T)}{\partial T} \quad (5)$$

Here, T and $L(T)$ indicate the temperature and length of the specimen at temperature. As expected, $Sc_2(WO_4)_3$ exhibits negative thermal expansion ($-5.82 \times 10^{-6}\,^{\circ}C^{-1}$) from room temperature to 600 °C, this result matches the report of Sleight et al. [14]. An almost constant negative thermal expansion coefficient ($-4.47 \times 10^{-6}\,^{\circ}C^{-1}$) was observed for $Sc_2W_3O_{12}$/Cu core–shell composite from room temperature to 200 °C, followed by an abrupt jump in the thermal expansion curve. Discrete difference of thermal expansion coefficient at 200 °C could be ascribed to the oxidation of copper. The specimen after TMA test takes on black color, and XRD and EDS analysis confirm that a new layer of CuO is created on the surface due to the oxidation of Cu crystallites. Unfortunately, the TMA used cannot test samples in inert gas atmosphere. The decrease in the CTE (from $-5.82 \times 10^{-6}\,^{\circ}C^{-1}$ to $-4.47 \times 10^{-6}\,^{\circ}C^{-1}$) is another evidence for Cu deposition on the $Sc_2W_3O_{12}$ surface as Cu shows positive thermal expansion ($17.7 \times 10^{-6}\,^{\circ}C^{-1}$). The CTE of the $Sc_2W_3O_{12}$/Cu core–shell composite could be adjusted to be negative, positive or even near zero just by controlling the thickness of the Cu shell. Moreover, this present synthesis method of synthesizing $Sc_2W_3O_{12}$/Cu core–shell composite shows an easy processing to attain the final product, which can be applied in a variety of fields, including metrology, precision optics, and space structures, and new functional device assemblies.

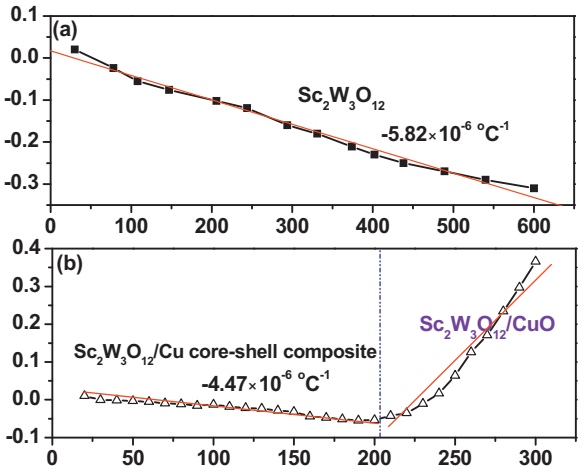

Fig. 3. Temperature dependence of linear thermal expansion of (a) the $Sc_2W_3O_{12}$ and (b) $Sc_2W_3O_{12}$/Cu core–shell composite.

4. Conclusion

In summary, the $Sc_2W_3O_{12}$/Cu composites have been successfully synthesized with the coating of copper layers on $Sc_2W_3O_{12}$ using electroless plating technique. A core–shell structure is constructed where the core is $Sc_2W_3O_{12}$ and Cu acts as the shell. The formation of catalytic of Pd–Sn core structure is a key factor to the construction of the $Sc_2W_3O_{12}$/Cu core–shell structure in the present electroless plating process, first, Pd–Sn catalytic core is believed to be adsorbed to $Sc_2W_3O_{12}$ surfaces after the sensitization and activation, followed by the deposition of nano-sized Cu crystallites on the Pd–Sn core surface and grew together to form continuous coating. The $Sc_2W_3O_{12}$/Cu composite with a density of about 5.13 g/cm^3 displays negative thermal expansion ($-4.47 \times 10^{-6}\,^{\circ}C^{-1}$) from room temperature to 200 °C due to the limit of the equipment.

Acknowledgement

This work was financially supported by the National Natural Science Foundation of China (No. 50772044) and the Doctoral Fund of Ministry of Education of China (No. 200802990001), Jiangsu University Development Foundation for Talents (No. 11JDG025) and China Postdoctoral Science Foundation (No. 20110491356).

References

[1] Th. Schubert, A. Brendel, K. Schmid, Th. Koeck, Ł. Ciupiński, W. Zieliński, T. Weißgärber, B. Kieback, Interfacial design of Cu/SiC composites prepared by powder metallurgy for heat sink applications, Composites A 38A (2007) 2398–2403.

[2] J. Tian, K. Shobu, Hot-pressed AlN-Cu metal matrix composites and their thermal properties, J. Mater. Sci. 39 (2004) 1309–1313.
[3] P. Yih, D.D.L. Chuang, Titanium diboride copper-matrix composites, J. Mater. Sci. 32 (1997) 1703–1709.
[4] Z.Y. Ma, S.C. Tjong, High temperature creep behavior of in-situ TiB2 particulate reinforced copper-based composite, Mater. Sci. Eng. A 284 (2000) 70–76.
[5] Z.W. Xue, Z. Liu, L.D. Wang, W.D. Fei, Thermal properties of new copper matrix composite reinforced by β-eucryptite particulates, Mater. Sci. Technol. 26 (2010) 1521–1524.
[6] A. Manna, B. Bhattacharyya, A study on different tooling systems during machining of Al/SiC-MMC, J. Mater. Process. Technol. 123 (2002) 476–482.
[7] I. Radu, D.Y. Li, Effects of ZrW_2O_8 and tungsten additions on the temperature range in which a pseudoelastic TiNi alloy retains its maximum wear resistance, Wear 263 (2007) 858–865.
[8] X.H. Yan, J. Qiu, C.S. Wang, C.H. Zhang, X.N. Cheng, Preparation of Cu coated ZrW_2O_8 composite powders via heterogeneous precipitation process, High Perform. Ceram. 368–372 (2008) 1377–1379.
[9] C. Verdon, D.C. Dunand, High-temperature reactivity in the ZrW_2O_8–Cu system, Scripta Mater. 36 (1997) 1075–1080.
[10] S. Yilmaz, D.C. Dunand, Finite-element analysis of thermal expansion and thermal mismatch stresses in a Cu–60 vol% ZrW_2O_8 composite, Compos. Sci. Technol. 64 (2004) 1895–1898.
[11] A.K.A. Pryde, K.D. Hammonds, M.T.V. Dove, J.D. Gale Heine, M.C. Warren, Origin of the negative thermal expansion in ZrW_2O_8 and ZrW_2O_7, J. Phys. Condens. Mat. 8 (1996) 10973–10982.
[12] S. Nishiyama, T. Hayashi, T. Hattori, Synthesis of ZrW_2O_8 by quick cooling and measurement of negative thermal expansion of the sintered bodies, J. Alloys Compd. 417 (2006) 187–189.
[13] J.S.O. Evans, T.A. Mary, A.W. Sleight, Negative thermal expansion in $Sc_2(WO_4)_3$, J. Solid State Chem. 137 (1998) 148–160.
[14] J.S.O. Evans, T.A. Mary, A.W. Sleight, Negative thermal expansion in a large molybdate and tungstate family, J. Solid State Chem. 133 (1997) 580–583.
[15] H. Gleiter, Materials with ultrafine microstructures: retrospectives and perspectives, Nanostruct. Mater. 1 (1992) 1–19.
[16] S.L. Zhu, L. Tang, Z.D. Cui, Q. Wei, X.J. Yang, Preparation of copper-coated β-SiC nanoparticles by electroless plating, Surf. Coat. Technol. 205 (2011) 2985–2988.
[17] S. Shukla, S. Seal, Z. Rahaman, K. Scammon, Electroless copper coating of cenospheres using silver nitrate activator, Mater. Lett. 57 (2002) 151–156.